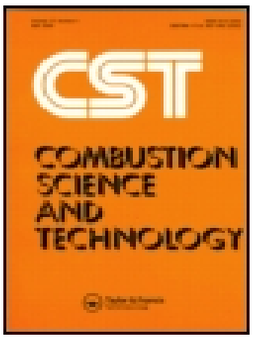

Combustion Science and Technology

ISSN: (Print) (Online) Journal homepage: https://www.tandfonline.com/loi/gcst20

Logistic-Regression-Based Meta-Analysis of Factors Affecting Flame Stability in a Shock Tube

Adam J. Susa, Alison M. Ferris, Lingzhi Zheng & Ronald K. Hanson

To cite this article: Adam J. Susa, Alison M. Ferris, Lingzhi Zheng & Ronald K. Hanson (2022): Logistic-Regression-Based Meta-Analysis of Factors Affecting Flame Stability in a Shock Tube, Combustion Science and Technology, DOI: 10.1080/00102202.2022.2142046

To link to this article: https://doi.org/10.1080/00102202.2022.2142046

COMBUSTION SCIENCE AND TECHNOLOGY
https://doi.org/10.1080/00102202.2022.2142046

Taylor & Francis
Taylor & Francis Group

Logistic-Regression-Based Meta-Analysis of Factors Affecting Flame Stability in a Shock Tube

Adam J. Susa, Alison M. Ferris, Lingzhi Zheng, and Ronald K. Hanson

Mechanical Engineering Department, Stanford University, Stanford, CA, USA

ABSTRACT

This work describes a meta-analysis performed in an effort to better understand the parameters controlling flame stability in shock-tube flame experiments. The data set used in the analysis was aggregated from multiple prior studies employing the shock-tube flame speed method, as well as previously unreported results. Flames are first qualitatively classified as being smooth, distorted, or wrinkled based on end-wall images. A subset of trials capturing the stability transition from stable to unstable flames are then selected from each set of experiments. Across all data sets, the transition between stable and unstable flames is analyzed as a binary classification problem using logistic regression. The resulting classification model, cast in terms of a multivariate power-law expression for the critical temperature (T_{crit}) at which flames become unstable, is found to be highly predictive of the stability transition. Consideration of the trained model coefficients allows the effects of different experimental parameters on T_{crit} to be identified. Model parameters provide significant new insight into the selection of diluents in experiments; the use of a test gas with a high heat capacity ratio is found to have the most beneficial effect toward increasing T_{crit}, while the effects of Lewis number and molecular weight are determined to be negligible. Ignition-location and pressure effects are less well quantified due to limited available data and are identified as key areas of further study.

ARTICLE HISTORY
Received 8 September 2022
Revised 01 November 2022
Accepted 27 October 2022

KEYWORDS
Shock tube; laminar flame speed; instability

Introduction

At the extreme conditions reached within modern combustion engines, flame propagation and spontaneous ignition chemistry can occur simultaneously, coupling with one another to jointly govern engine operability and performance (Puduppakkam et al. 2020). Efforts to predict the behavior of laminar flames at high unburned-gas temperatures at which the fuel – air mixture becomes spontaneously reactive have employed numerous simulation-based methods (*e.g.*, Sankaran 2015; Pan et al. 2016; Krisman, Hawkes, and Chen 2018; Ansari, Jayachandran, and Egolfopoulos 2019; Faghih et al. 2019; Zhang et al. 2020). However, while significant advancements have extended the range of pressures accessible to experimental laminar flame speed (S_L) measurement (*e.g.*, Tse, Zhu, and Law 2000; Xiouris et al. 2016), practical limitations have consistently hindered efforts to extend S_L measurements to higher temperatures.

CONTACT Adam J. Susa asusa@alumni.stanford.edu Building 570, Room 118 438 Panama Mall Stanford, CA, USA 94305

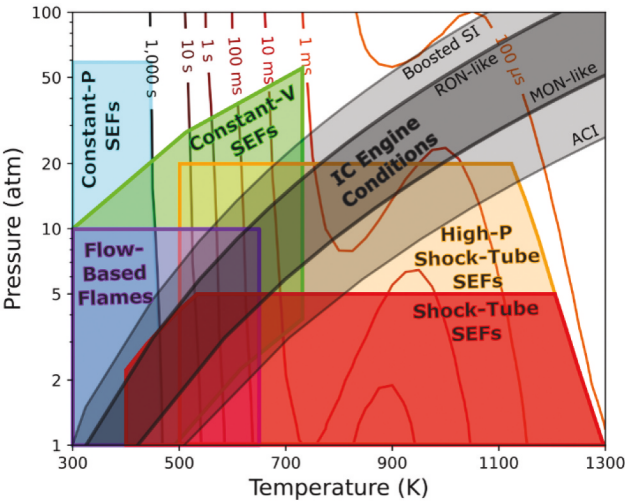

Figure 1. Temperature–pressure regime diagram comparing the approximate domains accessible to different S_L measurement approaches compared to an isentropic approximation of IC-engine-relevant conditions and IDT contours for *n* -heptane at $\phi = 1$.

The approximate unburned-gas temperature (T_u) and pressure (P_u) regimes accessible to different experimental approaches for the measurement of S_L are presented in Figure 1. Contours represent ignition delay times (IDTs) simulated for a stoichiometric (unity equivalence ratio, $\phi = 1$) mixture of *n* -heptane at constant pressure using a skeletal reaction mechanism from University of California at San Diego (2016). Conditions traditionally relevant to IC engines (dark gray) are shown bounded by air-standard isentropic trajectories from the research and motor octane number (RON and MON) intake conditions (ASTM D 2699: 2017–11 2017; ASTM D 2700: 2017–11 2017). An extended regime (light-gray) relevant to state-of-the-art engine technologies is shown bounded by isentropes originating from boosted spark ignition (SI) and advanced compression ignition (ACI) intake conditions (Szybist and Splitter 2020).

Flame speed measurements performed using constant-pressure (–P) spherically expanding flames (SEFs) can reach pressures as high as 60 atm (Tse, Zhu, and Law 2004), but are limited to low- T_u conditions by the long mixture residence time (on the order of 10 minutes) and are subject to fuel-loading constraints (Egolfopoulos et al. 2014). Constant-volume (–V), confined SEFs use dynamic heating of the unburned-gas mixture ahead of the flame to reach elevated temperatures. S_L measurements have been demonstrated up to 720 K using contemporary constant-V methods (Wang et al. 2020), with spontaneous autoignition of the preheated unburned gas limiting the ability of the method to reach higher T_u (Lawson et al. 2020). Flow-based flame speed measurements employing counterflow, Bunsen, or diverging-channel configurations use inline heating of the unburned gas to reach elevated temperatures. To the authors' knowledge, the 873-K data reported by Kurata, Takahashi, and Uchiyama (1994) using a Bunsen-flame configuration represent the highest-T_u S_L measurements reported in the literature prior to the introduction of the shock-tube flame speed method, though Bunsen flame data are often viewed as being subject to elevated uncertainty (Egolfopoulos et al. 2014). Heated, diverging channels have been employed in

S_L measurements up to about 650 K (*e.g.*, 2012). Rapid compression machines (RCMs) have been employed to measure burning velocities at T_u up to 1,000 K (*e.g.*, Assanis, Wagnon, and Wooldridge 2015); while flame wrinkling and pressure rise typically precludes the determination of S_L values from RCM experiments, recent progress realizing stable flames in RCMs has been reported at more moderate T_u conditions (Goyal and Samimi-Abianeh 2022).

The shock-tube flame speed method, first introduced by Ferris et al. (2019b), provides significant potential to enable S_L measurements at previously inaccessible T_u conditions (Figure 1). By pairing the ability of the shock-tube to nearly instantaneously heat an unburned-gas mixture with non-intrusive laser-induced ignition of a SEF and high-speed imaging diagnostics, the spontaneous-reactivity limits facing other S_L measurement methods can be overcome. The theoretical regime boundaries shown for shock-tube SEFs are described in (Susa 2022, 45–47). Despite this significant potential, early applications of the method (*e.g.*, Susa et al. 2019a, 2019b) were, in practice, limited by the occurrence of wrinkling, instability, and distortion of flames with increasing temperature. The schlieren-based propane measurements reported in Susa, Zheng, and Hanson (2021), performed using an oxidizer mixture of O_2 and Ar and with flames ignited much nearer the end wall than in previous studies, broke through these limits and demonstrated S_L measurements in excess of 1,000 K for the first time. Those results significantly expanded the demonstrated capability of the shock-tube flame speed method and motivate the present analysis of the factors that allowed that study to succeed.

This work describes a meta-analysis performed in an effort to better understand the parameters controlling flame stability in shock-tube flame experiments. The dataset used in the analysis was aggregated from multiple prior flame speed studies (Ferris et al. 2019a, 2019b; Ferris 2020a; Susa et al. 2019a; 2019b; Susa, Zheng, and Hanson 2021) as well as previously unreported results. The flame in each experiment is first classified by its stability, and a subset of trials capturing the transition from stable to unstable flames with increasing T_u is selected. The binary classification between stable and unstable is then analyzed using logistic regression. The resulting model, cast in terms of a multivariate power-law expression for the critical temperature (T_{crit}) at which flames become unstable, is found to be highly predictive of the stability transition. Consideration of the trained model coefficients allows the effects of different experimental parameters on the predicted stable T_u limit to be identified and informs the optimal design of future experiments.

Flame stability classifications

Flame stability is classified in this study by the subjective appearance of the flame at a characteristic diameter of approximately 3 cm. Flames are classified by three categories – stable ●, distorted ○, and wrinkled ☆ — selected to be analogous to those used in Susa et al. (2019a) and associated with a corresponding symbol used throughout this chapter. While the distorted and wrinkled categories are later lumped together to form the "unstable" binary class, they are distinguished in the classification phase to reflect the distinct appearances, illustrated by elevated-pressure propane–O_2/N_2/He flame images in Figure 2. The "distorted" name used to describe flames exhibiting concentric rings of emission is adopted from the side-wall imaging results of Susa and Hanson (2022) that found the rings seen in

Table 1. Experimental parameters.

Label	Fuel	Oxidizer				ϕ	P_5	γ_1	$\bar{M}$	$\bar{Le}$	z_5	T_5	Ref.
		O_2	N_2	He	Ar	(-)	(atm)	(-)	(g/mol)	(-)	(cm)	(K)	
CH_4-Air	CH_4	0.21	0.79	-	-	1.0	1.0	1.39	27.6	1.02	10.25	491–573	(Ferris et al. 2019b)
												582–607	(Ferris 2020b)
C_2H_6-Air	C_2H_6	0.21	0.79	-	-	1.0	1.0	1.38	28.9	1.20	10.25	459–534	(Ferris et al. 2019a)
												537–551	-
C_3H_8-Air	C_3H_8	0.21	0.79	-	-	1.0	1.0	1.37	29.5	1.35	10.25	496–556	(Ferris et al. 2019b)
												572-606	-
C_3H_8-He-2 atm	C_3H_8	0.21	0.32	0.47	-	1.0	2.0	1.44	18.6	2.48	10.25	488–587	-
C_3H_8-Ar	C_3H_8	0.21	-	-	0.79	1.0	1.0	1.51	38.5	1.26	10.25	547–826	-
C_3H_8-Ar-2 cm	C_3H_8	0.21	-	-	0.79	1.0	1.0	1.51	38.5	1.20	2.0	806–1,190	(Susa, Zheng, and Hanson 2021)
n -C_7H_{16}-Air	*n*-C_7H_{16}	0.21	0.79	-	-	0.9	1.0	1.36	30.1	2.27	10.25	401–595	(Susa et al. 2019b)
i-C_8H_{18}-Air	*i*-C_8H_{18}	0.21	0.79	-	-	0.9	1.0	1.36	30.1	2.33	10.25	502–594	(Susa et al. 2019b)
n -C_7H_{16}-He	*n*-C_7H_{16}	0.18	0.41	0.41	-	0.9	1.0	1.43	20.1	3.83	10.25	512–689	(Susa et al. 2019b)
i-C_8H_{18}-He	*i*-C_8H_{18}	0.18	0.41	0.41	-	0.9	1.0	1.43	20.1	4.00	10.25	505–641	(Susa et al. 2019a)

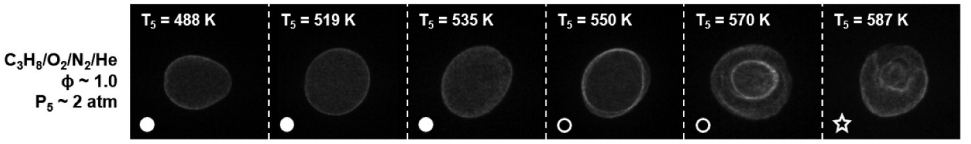

Figure 2. Propane–O_2/N_2/He flames ($\phi = 1.0$) at elevated pressure ($P_5 \approx 2$ atm). Symbols indicate the stability classification. Experiments represented in this figure are previously unpublished.

end-wall images to be associated with axial flame distortion. The nominal conditions of the 10 groupings of experiments included in the aggregate data set are detailed in Table 1; corresponding stability classifications vs. post-reflected-shock unburned-gas temperature (T_5) are presented in Figure 3.

It is noted that the radius used here to characterize flame stability is somewhat larger than the maximum radius required to perform a S_L measurement. As a result, flames at conditions classified as "unstable" in this chapter may, in fact, have been suitably stable for a reliable S_L measurement to be performed at smaller radii, as was the case for the methane, ethane, and propane experiments from Ferris et al. (2019a, 2019b) and Susa, Zheng, and Hanson (2021). In the cases of the *n*-heptane and *iso*-octane results (Susa et al. 2019a, 2019b), the presence of a fully stable radius range was less assured, such that axial flame distortion (Susa and Hanson 2022) is believed to have been a contributing factor to the observed negative temperature dependence reported in those experiments. Experiments from Ferris (2020b) were reported specifically for the purpose of illustrating the presence of non-ideal structure and thus not used in performing flame-speed measurements.

Analytical method

Logistic regression analysis is applied to estimate the extent to which different experimental parameters make a flame more or less prone to propagating in a stable manner. Logistic regression (Berkson 1944; Walker and Duncan 1967) is a method for estimating the value of

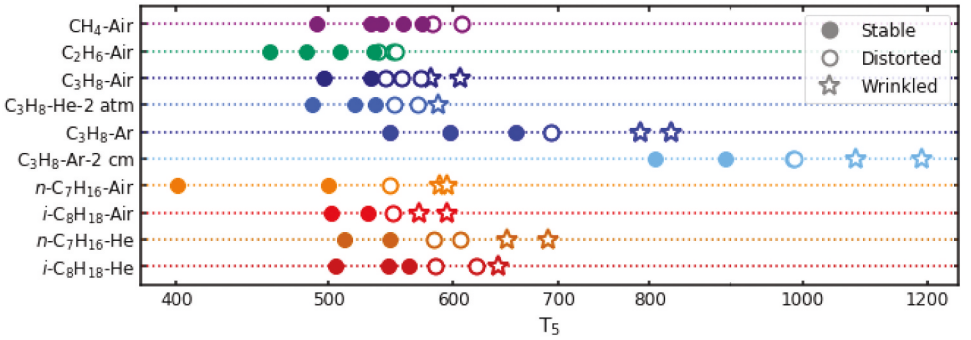

Figure 3. Stability of flames at different temperatures, T_5, grouped by experiment set. Each symbol represents a single shock-tube experiment, with the symbol shape corresponding to the stability classification. Y-axis labels correspond to those used in Table 1.

a binary dependent variable, y, from a set of n scalar independent variables, $\mathbf{x} = [1, x_1, x_2, \ldots, x_n]$; the $x_0 = 1$ feature is included to allow for a non-zero intercept. In the logistic model, the probability, P, of a given binary outcome, $y = 1$, given $\mathbf{x}$ is defined as:

$$P(y = 1|\mathbf{x}) = \sigma(t) = \frac{1}{1 + e^{-t}}, \tag{1}$$

$$t = \mathbf{B}\mathbf{x}^{\mathrm{T}} = \beta_0 + \beta_1 x_1 + \beta_2 x_2 + \ldots + \beta_n x_n = \sum_{i=0}^{n} \beta_i x_i, \tag{2}$$

where σ is the logistic function, t is a scalar value known as the "logit," and $\mathbf{B} = [\beta_0, \beta_1, \beta_2, \ldots, \beta_n]$ are a set of weights. Values of $t > 0$ are associated with the expected result that $y = 1$; $t < 0$ corresponds with an expectation of $y = 0$. In this work, the weights $\mathbf{B}$ are trained using a stochastic gradient descent (SGD) method (*i.e.*, SGDClassifier) implemented in the open-source Scikit-learn package (Pedregosa et al. 2011).

A typical shock-tube flame speed study consists of experiments performed over a range of T_5's while maintaining constant the other experimental parameters (pressure, mixture, *etc.*). Therefore, in order to predict the critical temperature (T_{crit}) at which a stable flame will no longer be realized in a given study, a power-law expression of the following form is sought:

$$T_{\mathrm{crit}} = cT_0 \prod_{i=2}^{n} \left(\frac{a_i}{a_{i,0}}\right)^{\theta_i} \begin{cases} > T_5, \text{ stable} \\ < T_5, \text{ unstable} \end{cases}, \tag{3}$$

where c is a constant and each independent parameter, a_i, non-dimensionalized by some characteristic value $a_{i,0}$, is taken to a power, θ_i, that defines the sensitivity of T_{crit} to that parameter. Letting $a_1 = T_5$, $a_{1,0} = T_0$, and $\theta_i = -1$, Eqn. 3 can be rewritten as:

$$c \prod_{i=1}^{n} \left(\frac{a_i}{a_{i,0}}\right)^{\theta_i} \begin{cases} > 1, \text{ stable} \\ < 1, \text{ unstable.} \end{cases} \tag{4}$$

Taking the natural logarithm converts Eqn. 4 into the form of a logit, t (Eqn. 2):

$$\ln(c) + \sum_{i=1}^{n} \theta_i \ln\left(\frac{a_i}{a_{i,0}}\right) = \ln(c) + \sum_{i=1}^{n} \theta_i (\alpha_i - \alpha_{i,0}) \begin{cases} > 0, & \text{stable} \\ < 0, & \text{unstable} \end{cases} = t, \tag{5}$$

where $\alpha_i \equiv \ln a_i$. SGD performs most reliably when the independent variables comprising $\mathbf{x}$ are standardized to zero mean and unit variance (scikit-learn developers n.d). Zero mean is realized for the $(\alpha_i - \alpha_{i,0})$ terms in Eqn. 5 if $\alpha_{i,0} = \mu_{\alpha,i}$, where $\mu_{\alpha,i}$ is the mean-log value of all values a_i in the training set. Division by the standard deviation, $s_{\alpha,i}$, of the α_i values enforces unit variance and is balanced by multiplying θ_i by $s_{\alpha,i}$:

$$t = \ln(c) + \sum_{i=1}^{n} (\theta_i s_{\alpha,i}) \left(\frac{\alpha_i - \mu_{\alpha,i}}{s_{\alpha,i}}\right). \tag{6}$$

Equation 6 is now exactly in the form of Eqn. 2, with:

$$\beta_0 = \ln(c), \tag{7}$$

$$\beta_{i\in\{1\ldots n\}} = \theta_i s_{\alpha,i}, \tag{8}$$

$$x_{i\in\{1\ldots n\}} = \frac{\alpha_i - \mu_{\alpha,i}}{s_{\alpha,i}}, \tag{9}$$

such that the parameters **B** trained on standardized features **x** can be interpreted as coefficients θ in the power-law form of Equation (3) and thus can provide physical insight into the factors affecting flame stability.

Results and discussion

Logistic regression was performed on the aggregate data set with the binary classifications of $y = 0$ assigned to stable flames and $y = 1$ assigned to both distorted and unstable flames. The resulting data set was closely balanced, containing 28 stable flames out of 61 total experiments. Six independent variables were selected to describe the experimental conditions: T_5 and P_5 characterize the thermodynamic state of the unburned gas; the room-temperature ratio of specific heats (γ_1), mixture-averaged molecular weight ($\bar{M}$), and Lewis number (Le) characterize the unburned-gas mixture; and the axial distance (z_5) from the end wall at which the flame is ignited characterizes the experimental configuration. Equivalence ratio is not independently considered in the present analysis as all available experiments were performed with ϕ near unity ($0.9 \leq \phi \leq 1.0$).

As SGD exhibits both sample-ordering and random-seed dependencies, a total of 200 training runs were performed using different seeds and ordering of the data. The mean and 95% confidence interval of each θ_i was calculated considering the 30 solutions producing the highest-scoring sets of weights, a process illustrated for θ_{γ_1} in Figure 4. Training results are tabulated for all θ_i coefficients in Table 2. Terms in the table correspond to an equation for T_{crit} of the following form, where $T_{\text{ref}} = cT_0$ and the units of dimensional quantities are specified:

$$T_{\text{crit}} = T_{\text{ref}} \left(\frac{P_5}{1.07\ \text{atm}}\right)^{\theta_{P_5}} \left(\frac{\gamma_1}{1.41}\right)^{\theta_{\gamma_1}} \left(\frac{\bar{M}}{27.4\ \text{g/mol}}\right)^{\theta_{\bar{M}}} \left(\frac{\text{Le}}{1.69}\right)^{\theta_{\text{Le}}} \left(\frac{z_5}{8.77\ \text{cm}}\right)^{\theta_{z_5}}. \tag{10}$$

The first row in Table 2 represents the results of the full, six-variable model, which scores 93% at predicting stability in the current data set using the average θ_i values. Outputs of the

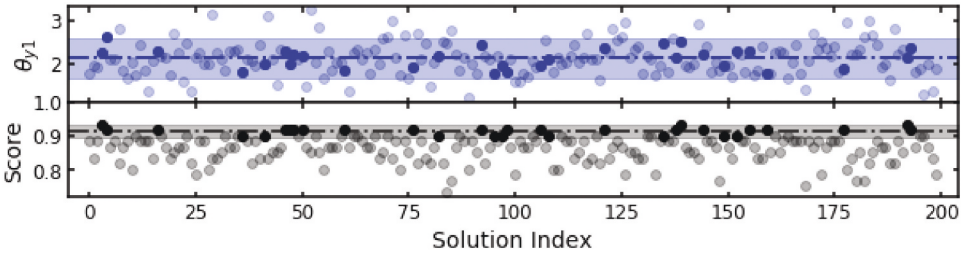

Figure 4. Coefficient θ_{γ_1} (top) and model score (bottom) resulting corresponding to 200 trained solutions. Mean values (dot-dash lines) and 95% confidence intervals (shaded regions) are calculated considering only the highest-scoring solutions (opaque symbols).

Table 2. Trained parameter values and confidence intervals.

Model	T_{ref} (K)	θ_{P_5}	θ_{γ_1}	$\theta_{\bar{M}}$	θ_{Le}	θ_{z_5}
Full	590 ± 9	−0.13 ± 0.10	2.14 ± 0.45	0.05 ± 0.05	−0.02 ± 0.03	−0.19 ± 0.04
Drop Le	588 ± 7	−0.12 ± 0.10	2.10 ± 0.39	0.05 ± 0.04	∅	−0.19 ± 0.05
Drop $\bar{M}$	586 ± 10	−0.15 ± 0.09	2.27 ± 0.49	∅	−0.04 ± −0.03	−0.18 ± 0.05

full model are displayed in Figure 5 in terms of both the logit, t, and the difference between the experimental and predicted critical temperatures, $T_5 - T_{crit}$. As neither θ_{Le} nor $\theta_{\bar{M}}$ are found to be statistically non-zero in the full model, two five-variable models are additionally considered, each dropping one of Le or $\bar{M}$ as independent variables. The "drop" model parameters are shown in the bottom two rows of the table; both matched the 93% score of the full model. It is found that when one of Le or $\bar{M}$ is dropped from the model, θ of the other becomes slightly statistically non-zero, such that one, but not both, of these parameters seems necessary in characterizing experimental conditions with respect to stability.

These empirical models provide insights into the experimental parameters affecting the stability limits in shock-tube flame experiments. The ratio of specific heats, γ_1, is found to be the parameter with the strongest effect, with larger values of γ_1 being beneficial to increasing T_{crit}. This strongly motivates the use of monatomic diluents (Ar and He, $\gamma = 5/3$) over diatomic nitrogen (N_2, $\gamma \approx 7/5$) for use in high-temperature flame experiments. It is further noted that the value θ_{γ_1} in these models reflects a weaker scaling than that applied to the closely related post-incident-shock ratio of specific heats ($\gamma_2^{-2.66}$) in an empirical expression describing the height of a reflected-shock bifurcation reported by Petersen and Hanson (2006). As such, at least one physical mechanism that could reasonably be expected to influence flame stability is known to exist that would explain a relationship of at least this magnitude.

While the strong correlation between γ_1 and stability motivates the use of Ar or He, it does not differentiate between the two. Furthermore, the nearly statistically nonexistent relationships between Le or $\bar{M}$ and stability do not provide a strong case for one over the other. Therefore, a different metric is required to identify the preferred diluent of Ar or He for experiments performed using the shock-tube flame speed method. The effect of the

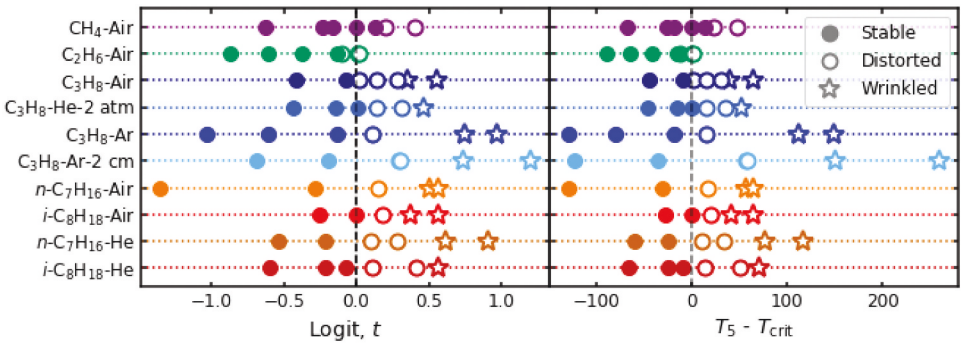

Figure 5. Results of the six-variable model applied to all data sets in term of the logit, t (left) and as the difference between T_5 and T_{crit} (right). Y-axis labels correspond to the labels in Table 1 and Figure 3. The vertical dashed lines represent the model predicted stability criteria. The modeled T_{crit} captures the stability transition (from filled to open symbols) across all experiment sets within about 20 K.

diluent selection on Le and the simulated S_L for a stoichiometric mixture of propane is shown in Figure 6. Viewing first the relationship between diluent selection and Le, it is seen that Le for mixtures diluted with Ar nearly exactly match those diluted with N_2, suggesting flames ignited in those mixtures would exhibit similar stretch responses. As N_2 is the air-relevant diluent for which data would generally be preferred by combustion practitioners, the use of Ar over He would be expected to provide more relevant data than early studies using He dilution with the shock-tube flame speed method (Ferris et al. 2019b; Susa et al. 2019a, 2019b) as well as many state-of-the-art S_L methods that use He dilution to suppress hydrodynamic instabilities (*e.g.* Rozenchan et al. 2002; Tse, Zhu, and Law 2004; Xiouris et al. 2016; Wang et al. 2020). Looking next to S_L, it can be seen that both monotonic diluents lead to an increase compared to N_2 on account of higher equilibrium temperatures. However, the increase seen using Ar is only about half that induced by He, once again making Ar-diluted mixtures more relevant to air than those containing He.

The axial position of the flame (z_5) exhibits the next strongest effect on the critical temperature. While the magnitude of θ_{z_5} is not particularly large, the wide range over which z_5 may be varied can nonetheless lead to a significant effect on T_{crit} predicted by the present model. This is observable in Figure 3 by comparing the baseline "C_3H_8-Ar" data set with the "C_3H_8-Ar-2 cm" data; reducing z_5 from 10.25 cm to 2 cm resulted in a significant increase in T_{crit}, from below 700 K to over 900 K. Based on the measurements reported in Susa and Hanson (2021) of axial velocity within the region-5 environment that is expected to increase in magnitude with distance from the end wall, this positional effect may be associated with igniting the flame in a more quiescent environment.

While z_5 clearly has some significant effect on flame stability, the magnitude and nature of the effect are made uncertain by the availability of only a single data set using a value z_5 other than 10.25 cm. For this reason, the identification and characterization of the specific mechanism underlying the positioning effect and are identified as a high-priority topic for further study. One preliminary study of positional effects was reported in Susa et al. (2022b), which revealed a more complex relationship between the position and stability than the simple, monotonic scaling

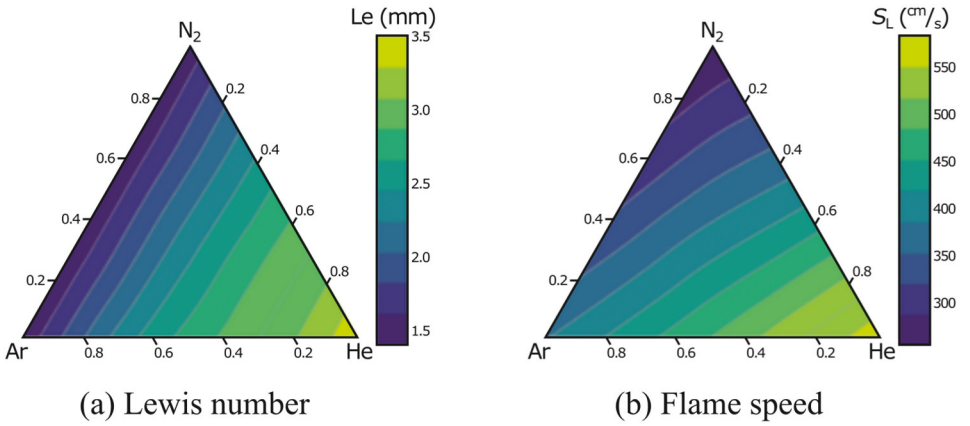

Figure 6. Ternary diagrams illustrating the effect of the diluent on (a) mixture Lewis number (Le), and (b) laminar flame speed (S_L) for propane ($\phi = 1$) in an oxidizer containing 21% O_2 and 79% diluent (N_2, Ar, He) at T_u = 800 K and P_u = 1 atm.

contained in the present analysis. For this reason, while the positional term in the present model might offer some general guidance, the authors urge caution in the model being assumed quantitatively predictive with respect to the positioning term.

The effect of unburned-gas pressure, P_5, is found to be small and uncertain. The uncertainty is attributed to only the single "C_3H_8-He-2 atm" data set being available at a pressure other than one atmosphere. Within the limits of the present model, it is expected that flames studied at higher pressure will experience a modest decrease in T_{crit}; for example, a 10-fold increase in pressure is predicted to result in a 22% decrease in T_{crit}. The magnitude of θ_{P_5} is strikingly similar to the pressure exponent of -0.14 associated with the analytical form of shock attenuation (Petersen and Hanson 2001), which could reflect a physical mechanism giving rise to the effect. However, further investigation is warranted to increase confidence in θ_{P_5} before conclusions regarding pressure effects can be drawn.

Conclusion

A regression-based meta-analysis of flame stability in a shock-tube environment was reported. A binary classifier was trained on an aggregate set of flame-stability data using SGD. The resulting model was cast as a power-law expression for predicting the critical temperature at which flames will become unstable in a shock tube, providing physical insight into the experimental parameters controlling flame stability. The strongest effect was found to be associated with γ_1, where increasing the value through the use of monatomic diluents promotes stability. Mixture Le and $\bar{M}$ were found to have negligible effect on T_{crit} in the limit of the Le >1 conditions evaluated in the present study; an evaluation of diluent effects on S_{L} and Le demonstrated that the use of Ar should be favored over He for maximizing the relevance to flames in air, as was used to good effect in a pair of recent studies (Susa et al. 2022a; Susa, Zheng, and Hanson 2022). The effect of z_5 is predicted by the model to be important but is uncertain on account of the limited availability of data and is identified as a topic of particular importance for further study. The effect of P_{u} is found to be relatively small but similarly uncertain; future applications of the shock-tube flame speed method at higher pressures will provide additional insight into the magnitude of the effect on flame stability.

Using this analytical framework and these preliminary results as guides, shock-tube flame speed experiments can now be designed to maximize the temperature range for stable flames, particularly through the informed selection of Ar as the diluent in the oxidizer. Future experiments designed using the present model as a guide will naturally interrogate the accuracy of the model parameters, and the incorporation of future results into an expanded aggregate data set will enable the predictive model to be iteratively refined over time. As additional experimental results become available to bolster and broaden the aggregate data set, further value could be realized by incorporating additional independent variables into the model, such as equivalence ratio. While the present model considers only a single flame radius, future analysis could treat the radius as an independent variable in order to predict T_{crit} at a specific radius of interest. Facility-specific parameters, including the radius of the shock tube, incident-shock attenuation rate, and T_1 (for heated shock tubes), may additionally be expected to affect T_{crit} and could become candidates for inclusion in future studies following this analysis methodology once results from other shock-tube facilities become available.

Acknowledgments

The authors thank Dr. Katherine Metcalf for discussions helpful to the selection and implementation of the logistic-regression classifier.

Disclosure statement

No potential conflict of interest was reported by the author(s).

Funding

The work was supported by the Army Research Office [W911NF-17-1-0420]; U.S. Department of Defense [NDSEG Fellowship (A.J. Susa)]; U.S. National Science Foundation [1940865]

ORCID

Adam J. Susa http://orcid.org/0000-0002-0094-869X
Alison M. Ferris http://orcid.org/0000-0002-5331-2812
Lingzhi Zheng http://orcid.org/0000-0003-4698-6357

Publication history

The contents of this paper are based on material included in the Ph.D. dissertation of A. J. Susa (Susa 2022, Ch. 5).

References

Akram, M., and S. Kumar. 2012. Measurement of laminar burning velocity of liquified petrolium gas air mixtures at elevated temperatures. *Energy Fuels* 26 (6):3267–74. doi:10.1021/ef300101n.

Ansari, A., J. Jayachandran, and F. N. Egolfopoulos. 2019. Parameters influencing the burning rate of laminar flames propagating into a reacting mixture. *Proc. Combust. Inst.* 37 (2):1513–20. doi:10.1016/j.proci.2018.05.163.

Assanis, D., S. W. Wagnon, and M. S. Wooldridge. 2015. An experimental study of flame and autoignition interactions of iso-octane and air mixtures. *Combust. Flame* 162 (4):1214–24. doi:10.1016/j.combustflame.2014.10.012.

ASTM D 2699: 2017-11. 2017. Test method for research octane number of spark-ignition engine fuel. Technical report. ASTM.

ASTM D 2700: 2017-11. 2017. Test method for motor octane number of spark-ignition engine fuel. Technical report. ASTM.

Berkson, J. 1944. Application of the logistic function to bio-assay. *J. Am. Stat. Assoc.* 39 (227):357–65. doi:10.1080/01621459.1944.10500699.

Egolfopoulos, F. N., N. Hansen, Y. Ju, K. Kohse-Höinghaus, C. K. Law, and F. Qi. 2014. Advances and challenges in laminar flame experiments and implications for combustion chemistry. *Prog. Energy Combust. Sci.* 43:36–67. doi:10.1016/j.pecs.2014.04.004.

Faghih, M., H. Li, X. Gou, and Z. Chen. 2019. On laminar premixed flame propagating into autoigniting mixtures under engine-relevant conditions. *Proc. Combust. Inst.* 37 (4):4673–80. doi:10.1016/j.proci.2018.06.058.

Ferris, A. M. 2020a. Development of fast-sampled species and laminar flame speed measurement techniques in a shock tube. PhD diss., Stanford University.

Ferris, A. M. 2020b. Non-ideal flame phenomenon: Multiple flame fronts? In *Chap. 6.5*, 183–88. Stanford University.

Ferris, A. M., J. J. Girard, A. J. Susa, D. F. Davidson, and R. K. Hanson. 2019a. Temperature, species, and laminar flame speed measurements in high-temperature, premixed ethane-air flames. In 11th US National Combustion Meeting, Pasedena, CA, USA.

Ferris, A. M., A. J. Susa, D. F. Davidson, and R. K. Hanson. 2019b. High-temperature laminar flame speed measurements in a shock tube. *Combust. Flame* 205:241–52. doi:10.1016/j.combustflame.2019.04.007.

Goyal, T., and O. Samimi-Abianeh. 2022. Methane laminar flame speed measurement at high gas temperature using rapid compression machine-flame (RCM-flame). *Ind. Eng. Chem. Res.* 61 (28):9981–90. doi:10.1021/acs.iecr.2c01117.

Krisman, A., E. R. Hawkes, and J. H. Chen. 2018. The structure and propagation of laminar flames under autoignitive conditions. *Combust. Flame* 188:399–411. doi:10.1016/j.combustflame.2017.09.012.

Kurata, O., S. Takahashi, and Y. Uchiyama. 1994. Influence of preheat temperature on the laminar burning velocity of methane-air mixtures. *SAE Trans.* 103:1766–72.

Lawson, R., V. Gururajan, A. Movaghar, and F. N. Egolfopoulos. 2020. Autoignition of reacting mixtures at engine-relevant conditions using confined spherically expanding flames. *Proc. Combust. Inst.* 38 (2):2285–93. doi:10.1016/j.proci.2020.06.224.

Pan, J., H. Wei, G. Shu, Z. Chen, and P. Zhao. 2016. The role of low temperature chemistry in combustion mode development under elevated pressures. *Combust. Flame* 174:179–93. doi:10.1016/j.combustflame.2016.09.012.

Pedregosa, F., G. Varoquaux, A. Gramfort, V. Michel, B. Thirion, O. Grisel, M. Blondel, et al. 2011. Scikit-learn: Machine learning in python. *J. Mach. Learn. Res.* 12:2825–30.

Petersen, E. L., and R. K. Hanson. 2001. Nonideal effects behind reflected shock waves in a high-pressure shock tube. *Shock Waves* 10 (6):405–20. doi:10.1007/PL00004051.

Petersen, E. L., and R. K. Hanson. 2006. Measurement of reflected-shock bifurcation over a wide range of gas composition and pressure. *Shock Waves* 15 (5):333–40. doi:10.1007/s00193-006-0032-3.

Puduppakkam, K. V., A. U. Modak, C. Wang, D. Hodgson, C. V. Naik, and E. Meeks. 2020. Generating laminar flame speed libraries for autoignition conditions. In *Turbo expo: Power for land, sea, and air*, Vol. 84133, ASME. doi:10.1115/GT2020-15274.

Rozenchan, G., D. L. Zhu, C. K. Law, and S. D. Tse. 2002. Outward propagation, burning velocities, and chemical effects of methane flames up to 60 atm. *Proc. Combust. Inst.* 29 (2):1461–70. doi:10.1016/S1540-7489(02)80179-1.

Sankaran, R. 2015. Propagation velocity of a deflagration front in a preheated autoigniting mixture. In 9th US Natlonal Combustion Meeting, Cincinnati, OH, USA.

scikit-learn developers. n.d. Sklearn.Linear_model.sgdclassifier. https://scikit-learn.org/stable/modules/generated/sklearn.linear_model.SGDClassifier.html.

Susa, A. J. 2022. High-speed imaging studies of flames in a shock tube: refined techniques and new applications. PhD diss., Stanford University.

Susa, A. J., A. M. Ferris, D. F. Davidson, and R. K. Hanson. 2019a. Experimental observation of negative temperature dependence in iso-octane burning velocities. *AIAA J.* 57 (10):4476–81. doi:10.2514/1.J058530.

Susa, A. J., A. M. Ferris, D. F. Davidson, and R. K. Hanson. 2019b. Experimental shock tube measurements of laminar burning velocity of n-heptane and iso-octane in the negative temperature coefficient regime AIAA Scitech 2019 Forum, San Diego, CA, USA, 0460. American Institute of Aeronautics and Astronautics. doi:10.2514/6.2019-0460.

Susa, A. J., and R. K. Hanson. 2021. Flame-drift velocimetry and flame morphology measurements with dual-perspective imaging in a shock tube. *12th US Natl. Combust. Meet* 1G13.

Susa, A. J., and R. K. Hanson. 2022. Distortion of expanding n-heptane flames at high unburned-gas temperatures behind reflected shocks. *Combust. Flame* 237:111842. doi:10.1016/j.combustflame.2021.111842.

Susa, A. J., L. Zheng, and R. K. Hanson. 2021. Schlieren-based measurements of propane flame speeds at extreme temperatures. In 12th US National Combustion Meeting, Virtual and College Station, TX, USA, 1G05.

Susa, A. J., L. Zheng, and R. K. Hanson. 2022. Measurements of propane-O_2-Ar laminar flame speeds at temperatures exceeding 1000 K in a shock tube, *Proceedings of the Combustion Institute*. doi:10.1016/j.proci.2022.07.191

Susa, A. J., L. Zheng, Z. D. Nygaard, A. M. Ferris, and R. K. Hanson. 2022a. Laminar flame speed measurements of primary reference fuels at extreme temperatures. In Proceedings of the ASME 2022 Internal Combustion Engine Division Fall Technical Conference (ICEF2022) Indianapolis, IN, USA, ICEF2022–90501.

Susa, A. J., L. Zheng, Z. D. Nygaard, and R. K. Hanson. 2022b. End-wall effects on freely propagating flames in a shock tube, AIAA Scitech 2022 Forum, San Diego, CA, USA, 2346. American Institute of Aeronautics and Astronautics.

Szybist, J. P., and D. A. Splitter. 2020. Impact of engine pressure-temperature trajectory on autoignition for varying fuel properties. *Appl. Energy Combust. Sci.* 1-4:100003. doi:10.1016/j.jaecs.2020.100003.

Tse, S. D., D. L. Zhu, and C. K. Law. 2000. Morphology and burning rates of expanding spherical flames in H2/O2/inert mixtures up to 60 atmospheres. *Proc. Combust. Inst.* 28 (2):1793–800. doi:10.1016/S0082-0784(00)80581-0.

Tse, S. D., D. L. Zhu, and C. K. Law. 2004. Optically accessible high-pressure combustion apparatus. *Rev . Sci. Instrum.* 75 (1):233–39. doi:10.1063/1.1634358.

University of California at San Diego. 2016. *Chemical-Kinetic Mechanisms for Combustion Applications*.

Walker, S. H., and D. B. Duncan. 1967. Estimation of the probability of an event as a function of several independent variables. *Biometrika* 54 (1–2):167. doi:10.1093/biomet/54.1-2.167.

Wang, Y., A. Movaghar, Z. Wang, Z. Liu, W. Sun, F. N. Egolfopoulos, and Z. Chen. 2020. Laminar flame speeds of methane/air mixtures at engine conditions: Performance of different kinetic models and power-law correlations. *Combust. Flame* 218:101–08. doi:10.1016/j.combustflame.2020.05.004.

Xiouris, C., T. Ye, J. Jayachandran, and F. N. Egolfopoulos. 2016. Laminar flame speeds under engine-relevant conditions: Uncertainty quantification and minimization in spherically expanding flame experiments. *Combust. Flame* 163:270–83. doi:10.1016/j.combustflame.2015.10.003.

Zhang, T., A. J. Susa, R. K. Hanson, and Y. Ju. 2020. Studies of the dynamics of autoignition assisted outwardly propagating spherical cool and double flames under shock-tube conditions. *Proc. Combust. Inst.* 38 (2):2275–83. doi:10.1016/j.proci.2020.06.089.